

Observation of Structure Evolution and Reaction Intermediates at the Gate-tunable Suspended Graphene/Electrolyte Interface

Ying Xu¹, You-Bo Ma¹, Feng Gu¹, Shan-Shan Yang¹, Chuan-Shan Tian^{1,2*}

¹Department of Physics, State Key Laboratory of Surface Physics and Key Laboratory of Micro- and Nano-Photonic Structures (MOE), Fudan University; Shanghai, 200433, China.

² Collaborative Innovation Center of Advanced Microstructures; Nanjing, 210093, China.

*Corresponding author. Email: cstian@fudan.edu.cn

Abstract: Graphene serves as an ideal platform to investigate the microscopic structure and reaction kinetics at the graphitic electrode interfaces. However, graphene is susceptible to various extrinsic factors, e.g. substrate, causing much confusion and controversy. Hereby we have obtained cm-sized substrate-free monolayer graphene suspended on electrolyte surface with gate tunability. Using sum-frequency spectroscopy, we have observed the structural evolution versus the gate voltage at the graphene/water interface. The Stern layer structure is invariant within the water electrolysis window, but undergoes drastic change when switching on the electrochemical reactions. The electrode is turned from hydrophobic to hydrophilic near the onset of hydrogen evolution reaction due to hydrogen adsorption. The large-size suspended pristine graphene offers a new platform to unravel the microscopic processes at the graphitic electrode interfaces.

Graphitic electrode is commonly used in electrochemical reactions due to its excellent in-plane conductivity, structural robustness and cost-efficiency^{1,2}. It serves as prime electrocatalyst support as well as a layered intercalation matrix²⁻⁴ with wide applications in energy conversion and storage, such as fuel cells, electrolysis hydrogen generation, and lithium-ion batteries^{1,5,6}. Understanding these electrochemical processes requires molecular-level knowledge of the structure, and the intermediate and product species at the graphitic electrode interface during the reaction. However, such information remains limited thus far, hampered by the difficulties in probing the solid-liquid interface in a practical environment^{7,8}. Over the past decades, chemical-sensitive optical spectroscopic techniques combined with cyclic-voltammetry (CV) have been developed to investigate buried electrochemical interfaces⁹⁻¹¹. Unfortunately, most of them suffer from either poor surface sensitivity or strong attenuation when the probe beams pass through the electrode or electrolyte to access the interface⁹⁻¹¹. On the other hand, being the two-dimensional building block of graphite, graphene shares similar chemical properties with graphite^{1,2,12}, while its unique physical and chemical properties offer more varieties and tunability for developing state-of-the-art graphitic devices¹³⁻¹⁶. For instance, the chemisorption of atomic hydrogen on a graphene sheet has been demonstrated as a promising route for efficient hydrogen storage at a low cost^{6,17,18}. More importantly, with monolayer thickness, the graphene/electrolyte interface is easily accessible by various optical and electron probes through graphene. Thus, with the help of surface-specific techniques^{13,14,19}, such as sum-frequency spectroscopy, the graphene/electrolyte interface provides an ideal platform to investigate the graphitic electrode interface during electrochemical reactions.

Despite the apparent advantages mentioned above and intensive studies, our current knowledge of the molecular structure at the interface between graphene electrode and the aqueous solution remains elusive or controversial in literature^{15,19-21}. The difficulty lies in the

fact that the fingerprints of the interfacial species are vulnerable to many extrinsic factors, such as the hydrophobicity of the substrate used to support graphene, as well as surface charge due to defects or band bending at the interface. For instance, theoretical calculations predicted graphene is hydrophobic, and the dangling O-H bond of water molecules protruding at the graphene/water interface is expected^{21,22}. However, earlier experiments could not observe its spectroscopic fingerprints^{19,23}. This contradiction had been attributed to the substrate, because the hydrophobicity is strongly affected by the substrate, known as the wetting transparency of graphene^{20,24}. Recently, Montenegro *et al* reported their observation of dangling O-D mode at CaF₂/graphene/D₂O interface¹⁵. Nevertheless, their conclusion remains questionable as the voltage applied on graphene is well beyond the water electrolysis window which raises the concern about the gaseous H₂ layer accumulated at the interface¹⁵. Meanwhile, existence of the substrate can significantly change the interfacial potential due to its surface chemistry or band bending^{19,25}, which would strongly affect the hydrogen-bond network of the interfacial water molecules. Therefore, a clean and substrate-free graphene electrode is urgently needed to unravel the intrinsic structural evolution as well as adsorption and accumulation of the intermediate and product species at the interface during electrochemical reactions, e.g. chemisorption of atomic hydrogen on graphene during hydrogen evolution reaction (HER)^{6,17,18}. In this work, we have obtained centimeter-sized substrate-free monolayer graphene (MLG) sheet on aqueous electrolyte surface using a newly developed transfer scheme for CVD graphene. At such MLG electrode/electrolyte interface, we have studied the molecular structure in the Stern layer as a function of the gate voltage, using sum-frequency vibrational spectroscopy (SFVS) combined with CV measurement.

The copper substrate of CVD graphene was etched away by electrolysis, as illustrated in Fig. 1(A). Then the electrolyte (0.3 M CuSO₄) solution in the cell was diluted by pure water

repeatedly to reduce the concentration of the unwanted ions (Cu^{2+} , SO_4^{2-}) to be less than 1 μM , with the MLG sample kept suspended on the surface of solution in the cell during the whole process (see Sec. A in Supplementary Materials (SM)). Finally, supporting electrolyte was added to water, and here we used KCl solution (0.1 M). The MLG suspended on the solution is about 6 mm \times 10 mm in size, as shown in Fig. 1 (B). Optical microscope image (Fig. 1 (C)) shows that the CVD-grown graphene sheet is intact without folding or shrinkage in the mesoscopic scale. Furthermore, the ratio of D-mode and G-mode I_D/I_G in Raman spectrum (Fig. 1 (D)) is about 1:8 and is essentially the same for graphene as-grown on copper substrate and graphene suspended on the solution, indicating that few lattice defects exist on graphene and that our fabrication process did not introduce additional defects^{26,27}. These results manifest the premium quality of our free-standing MLG sample.

We next explored the electrical tunability of the graphene/electrolyte interface. As illustrated in Fig. 2 (A), thin Pt wires (20 μm in diameter) were put in contact with the MLG sheet, benefitting from the superior mechanical strength of graphene²⁸. The graphene was used as the working electrode and a piece of Pt foil was immersed in the electrolyte as the counter electrode (Fig. 2 (A)), while Ag/AgCl in saturated KCl solution was used as the reference electrode. All of the voltages presented in this paper is referenced to Ag/AgCl (see Sec. A in SM). We first performed cyclic voltammetry (CV) measurement on the sample (scan rate 100 mV/s) and compared the result with that obtained on highly orientated pyrolytic graphite (HOPG) electrode (Fig. 2 (B)). The response of graphene is essentially the same as that of graphite. The water electrolysis window of our MLG sample is located between +1.0 V and -0.2 V. In this potential range, no chemical reaction occurs and a stable electric double layer (EDL) form upon applying voltage and the total surface charge density (σ) can be tuned continuously. Note that σ is different from the carrier density (n) in graphene because the graphene is generally doped

when in contact with aqueous solution. According to the quantum capacitance model of graphene²⁹ and the EDL model at the graphene/electrolyte interface³⁰ (also see section B in SM), n and σ can be readily deduced with known Dirac point and the potential of zero charge (pzc, where $\sigma = 0$) of the interface. To characterize the Dirac point, following the protocols in refs^{26,31}, we measured the frequency shift of Raman G mode and the in-plane resistance of graphene at different gate voltage V_G . As shown in Fig. 2 (C) and (D), the Fermi level is at the Dirac point when $V_G = -0.15$ V, as the resistance reaches maximum while frequency of G mode is at minimum. Pzc of the MLG/water interface was found to be 0.5 ± 0.1 V (see Sec. E in SM), which is close to that on HOPG basal plane reported in literature³².

With this gate-tunable pristine MLG/electrolyte interface, we have studied the interfacial water structure using phase-sensitive SFVS (experiment details given in Sec. C in SM)³³. Here, the stretching vibrations of water molecules (ranging from 3000 cm^{-1} to 3800 cm^{-1}) at the interface are resonantly excited by the frequency-tunable IR laser pulses during the sum-frequency generation (SFG) process. The resonant feature of the 2nd-order nonlinear response $\chi^{(2)}(\omega_R)$, obtained from the collected SF signal, can be used to derive the interfacial water structure in EDL. As a reference of a water interface, Fig. 3(A) shows the imaginary part of $\chi^{(2)}(\omega_R)$ spectrum at air/water interface³⁴, which directly characterizes the resonances. Being a hydrophobic interface, the spectrum generally consists of a broad continuum band from 3000 cm^{-1} to 3500 cm^{-1} and a narrow positive peak at 3700 cm^{-1} . The former is attributed to the hydrogen-bonded O-H vibrations, and the latter to the vibration of the dangling O-H bond protruding at the top-most layer as depicted in the inner plot of Fig. 3(A)^{35,36}. With MLG placed on the water surface (air/MLG/water interface), the $\text{Im}\chi^{(2)}$ spectrum changes significantly as shown in Fig. 3(A). The spectrum recorded at $V_G = 0$ V is also composed of two main resonant features as well

as a negative background (dashed line in Fig. 3(A)). Unambiguously, the dangling O-H band can now be observed at the pristine MLG/water interface, signifying the hydrophobic nature of graphene. The dangling OH mode is red-shifted by $\sim 100 \text{ cm}^{-1}$ with broader linewidth versus the counterpart at the air/water interface resulting from the interaction between dangling O-H bond and graphene, in good agreement with theoretical prediction²¹. Such O-H mode persists when V_G is tuned from 1.0 V to -0.2 V as evidenced in Fig. 3(B). It means the interface remains hydrophobic in the water electrolysis window. Meanwhile, the $\text{Im}\chi^{(2)}$ spectrum shows strong dependence on the gate voltage in the bonded O-H band between $3000\text{-}3500 \text{ cm}^{-1}$ and the negative background. In order to understand the evolution of the O-H spectrum and the background, we need to quantitatively analyze the origin of $\chi^{(2)}$ at this interface.

As illustrated in Fig. 3 (C), the total second-order nonlinear susceptibility ($\chi^{(2)}$) from the graphene/electrolyte interface contains three origins^{37,38}:

$$\chi^{(2)} = \chi_s^{(2)} + \chi_g^{(2)} + \chi^{(3)}\Psi \quad (1)$$

Here, $\chi_s^{(2)}$, $\chi_g^{(2)}$ and $\chi^{(3)}\Psi$ corresponds to the SF response from the Stern layer, graphene and the diffuse layer, respectively. Firstly, the Stern layer is composed of water molecules and ions that are closely packed near the electrode, and its structure is directly related to the energy and charge transfer across the interface during electrochemical reactions^{39,40}. Hence, $\chi_s^{(2)}$ that characterizes the microscopic structure of the Stern layer is what we are interested in the most. Secondly, the electric quadrupole and magnetic dipole responses of the free carriers in graphene account for the negative background ($\chi_g^{(2)}$) in the observed spectrum plotted in Fig. 3(B)^{38,41}. Knowing the Fermi level μ of graphene (relative to the Dirac point), $\chi_g^{(2)}$ can be calculated using the theory developed by the pioneering works^{38,41,42}. Finally, water molecules in the diffuse layer polarized by the screening electric field would generate SF signal proportional to $\chi^{(3)}\Psi$ (see ref³⁷ and

section E in SM). Here, $\chi^{(3)}$ is the 3rd-order responses of bulk water, and Ψ is the modified electric potential difference across the diffuse layer³⁷. It is sensitive to the charge density at the interface and could contribute significantly to the SF spectra in the bonded-OH band (3000 - 3500 cm^{-1}) given in Fig. 3(B).

In order to obtain $\text{Im}\chi_s^{(2)}$, we need to separate $\text{Im}\chi_g^{(2)}$ and $\text{Im}\chi^{(3)}\Psi$ from the measured $\text{Im}\chi^{(2)}$. We first evaluate $\text{Im}\chi_g^{(2)}$ by theoretical calculation using the formulism given in ref³⁸ and compare it with that measured at 3800 cm^{-1} , where the SF signals from $\chi_s^{(2)}$ and $\chi^{(3)}\Psi$ are off-resonance and negligibly small. As shown in Fig. 3(D), excellent agreement is achieved between the theoretical and experimental values as a function of the chemical potential μ of graphene. To the best of our knowledge, this is the first quantitative experimental verification of SF response versus μ on graphene. Having confirmed the theoretical results, we can obtain the $\text{Im}\chi_g^{(2)}$ spectrum between 3000 – 3800 cm^{-1} , as presented in Fig. 3(E). As expected, the calculated $\text{Im}\chi_g^{(2)}$ spectrum fits well with the background of the measured spectra in Fig. 3(B) at all gate voltages (see Section E in SM for details).

As for the contribution from the diffuse layer, based on the method established in our previous work, the $\text{Im}\chi^{(3)}$ spectrum of water has been already obtained³⁷ and Ψ can be deduced knowing the surface charge density σ and the ion concentration . Fig. 3(F) shows the calculated $\text{Im}\chi^{(3)}\Psi$ spectra at different V_G . Through comparison of the two sets of spectra in Fig. 3(B) and 3(F), the sign flip of the bonded O-H band in the measured $\text{Im}\chi^{(2)}$ as V_G is tuned from +1.0V to -0.2V is originated from the $\text{Im}\chi^{(3)}\Psi$ contribution when the electric field direction reverses in the diffuse layer.

The Stern layer spectrum ($\text{Im}\chi_s^{(2)}$) can now be obtained by subtracting the contributions of graphene and the diffuse layer from the measured SF spectra using Eq. (1). A contour plot of the $\text{Im}\chi_s^{(2)}$ spectrum at different V_G is presented in Fig. 3(G), with a few representative curves given in Fig. 4(A). Surprisingly, although the total SF spectrum (see Fig. 3(B)) changes significantly with V_G , the Stern layer spectrum is essentially independent of V_G between +0.7 V and 0.0 V, except for shift of the dangling OH band. It means the water structure close to graphene is hardly altered by the gate voltage within the water electrolysis window. The frequency shift of the dangling OH mode is the result of the vibrational Stark effect^{43,44}. In Fig. 4(B), we fitted the frequency shift $\Delta\nu$ versus the electric field E_s (positive if pointing towards graphene, see Section B in SM) in the Stern layer using the linear Stark effect:

$$\Delta\nu = -\alpha \cdot E_s \quad (2)$$

Here α is the Stark tuning rate. From the linear fit in Fig. 4 (A), $\alpha = 7 \pm 2 \text{ cm}^{-1}/\text{MV} \cdot \text{cm}^{-1}$, close to the theoretical value of $\alpha = 4.8 \text{ cm}^{-1}/\text{MV} \cdot \text{cm}^{-1}$ for water clusters in literature⁴³.

Knowing the Stern layer is invariant within the water electrolysis window, we further explored the microscopic structure at the pristine graphene/electrolyte interface by switching on the electrochemical reactions. As shown in Fig. 4(A), when the gate voltage is near the onset of electrolysis of water, namely at $V_G = 1.0 \text{ V}$ and -0.2 V , the bonded O-H band starts to change drastically. This indicates that the hydrogen-bond network has been strongly altered upon starting the chemical reactions. If we further lower the gate voltage down to -0.4 V , which is slightly beyond the threshold of HER, the dangling O-H mode disappears completely (Fig. 4(C)). The disappearance of the dangling O-H manifests that topmost layer of the interfacial water is strongly disturbed. In particular, the electrode has been turned from hydrophobic to hydrophilic⁴⁵. Meanwhile, the CV curves in Fig. 4(D) measured immediately after holding V_G at -0.4 V for

~4 hours show a peak at 0.3 V, and the peak current reduces after each loop. The peak at 0.3V indicates an irreversible desorption process of the products on graphene. Atomic H or molecular H₂ may be produced at the interface when V_G = -0.4 V. However, gaseous H₂ molecules at the interface should favor existence of the dangling O-H bond in analogy to the air/water interface¹⁵, rather than suppressing of the dangling O-H. Thus, the change of hydrophobicity of the electrode should be attributed to atomic H adsorbed on graphene prohibits dangling-like O-H at the interface, as illustrated in Fig. 4 (E). We note that in a recent published work, He *et al* also observed the signature of chemisorbed hydrogen atom on graphene at the onset of HER¹⁸.

In summary, our work demonstrated that substrate-free pristine graphene is essential for unraveling the intrinsic microscopic structure at the graphene electrode interface. The suspended graphene can be easily decorated with electro-catalysts, e.g. Pt and Au nanoparticles^{46,47}, to promote the electrochemical reactions. Thus, the large-size substrate-free MLG with superior mechanical strength and electrical tunability provides us an ideal platform for investigation of the interfacial species and their reaction kinetics at the graphitic electrode/electrolyte interface in general.

References

- 1 Das, R. K. *et al.* Extraordinary hydrogen evolution and oxidation reaction activity from carbon nanotubes and graphitic carbons. *Acs Nano* **8**, 8447-8456 (2014).
- 2 Murthy, A. P., Madhavan, J. & Murugan, K. Recent advances in hydrogen evolution reaction catalysts on carbon/carbon-based supports in acid media. *Journal of Power Sources* **398**, 9-26 (2018).
- 3 Enoki, T., Suzuki, M. & Endo, M. *Graphite intercalation compounds and applications*. (Oxford University Press, 2003).
- 4 Kibsgaard, J. *et al.* Cluster– support interactions and morphology of MoS₂ nanoclusters in a graphite-supported hydrotreating model catalyst. *Journal of the American Chemical Society* **128**, 13950-13958 (2006).
- 5 Kjeang, E., McKechnie, J., Sinton, D. & Djilali, N. Planar and three-dimensional microfluidic fuel cell architectures based on graphite rod electrodes. *Journal of Power Sources* **168**, 379-390 (2007).
- 6 Bonaccorso, F. *et al.* Graphene, related two-dimensional crystals, and hybrid systems for energy conversion and storage. *Science* **347**, 1246501 (2015).
- 7 Tripathi, A. M., Su, W.-N. & Hwang, B. J. In situ analytical techniques for battery interface analysis. *Chemical Society Reviews* **47**, 736-851 (2018).
- 8 Ye, S. in *Compendium of Surface and Interface Analysis* 79-85 (Springer, 2018).

- 9 Tian, Z. Q. & Ren, B. Adsorption and reaction at electrochemical interfaces as probed by surface-enhanced Raman spectroscopy. *Annual Review of Physical Chemistry* **55**, 197-229, doi:10.1146/annurev.physchem.54.011002.103833 (2004).
- 10 Richey, F. W., Dyatkin, B., Gogotsi, Y. & Elabd, Y. A. Ion dynamics in porous carbon electrodes in supercapacitors using in situ infrared spectroelectrochemistry. *Journal of the American Chemical Society* **135**, 12818-12826 (2013).
- 11 Liu, W.-T. & Shen, Y. R. In situ sum-frequency vibrational spectroscopy of electrochemical interfaces with surface plasmon resonance. *Proceedings of the National Academy of Sciences* **111**, 1293-1297 (2014).
- 12 Danaee, I. & Noori, S. Kinetics of the hydrogen evolution reaction on NiMn graphite modified electrode. *International Journal of Hydrogen Energy* **36**, 12102-12111 (2011).
- 13 Bie, Y.-Q. *et al.* Vibrational spectroscopy at electrolyte/electrode interfaces with graphene gratings. *Nature Communications* **6**, 1-6 (2015).
- 14 Peng, Q., Chen, J., Ji, H., Morita, A. & Ye, S. Origin of the overpotential for the oxygen evolution reaction on a well-defined graphene electrode probed by in situ sum frequency generation vibrational spectroscopy. *Journal of the American Chemical Society* **140**, 15568-15571 (2018).
- 15 Montenegro, A. *et al.* Asymmetric response of interfacial water to applied electric fields. *Nature* **594**, 62-65 (2021).
- 16 Yu, Y. *et al.* Tunable angle-dependent electrochemistry at twisted bilayer graphene with moiré flat bands. *Nature Chemistry* **14**, 267-273 (2022).
- 17 Pumera, M. Graphene-based nanomaterials for energy storage. *Energy & Environmental Science* **4**, 668-674, doi:10.1039/c0ee00295j (2011).
- 18 He, Q. *et al.* Electrochemical Storage of Atomic Hydrogen on Single Layer Graphene. *Journal of the American Chemical Society* **143**, 18419-18425 (2021).
- 19 Dreier, L. B. *et al.* Surface-specific spectroscopy of water at a potentiostatically controlled supported graphene monolayer. *The Journal of Physical Chemistry C* **123**, 24031-24038 (2019).
- 20 Rafiee, J. *et al.* Wetting transparency of graphene. *Nature Materials* **11**, 217-222 (2012).
- 21 Ohto, T., Tada, H. & Nagata, Y. Structure and dynamics of water at water-graphene and water-hexagonal boron-nitride sheet interfaces revealed by ab initio sum-frequency generation spectroscopy. *Physical Chemistry Chemical Physics* **20**, 12979-12985 (2018).
- 22 Zhang, Y., de Aguiar, H. B., Hynes, J. T. & Laage, D. Water structure, dynamics, and sum-frequency generation spectra at electrified graphene interfaces. *The Journal of Physical Chemistry Letters* **11**, 624-631 (2020).
- 23 Singla, S. *et al.* Insight on structure of water and ice next to graphene using surface-sensitive spectroscopy. *ACS nano* **11**, 4899-4906 (2017).
- 24 Prydatko, A. V., Belyaeva, L. A., Jiang, L., Lima, L. M. & Schneider, G. F. Contact angle measurement of free-standing square-millimeter single-layer graphene. *Nature Communications* **9**, 1-7 (2018).
- 25 Achtyl, J. L. *et al.* Aqueous proton transfer across single-layer graphene. *Nature Communications* **6**, 1-7 (2015).
- 26 Beams, R., Cançado, L. G. & Novotny, L. Raman characterization of defects and dopants in graphene. *Journal of Physics: Condensed Matter* **27**, 083002 (2015).
- 27 Eckmann, A. *et al.* Probing the nature of defects in graphene by Raman spectroscopy. *Nano letters* **12**, 3925-3930 (2012).
- 28 Frank, I., Tanenbaum, D. M., van der Zande, A. M. & McEuen, P. L. Mechanical properties of suspended graphene sheets. *Journal of Vacuum Science & Technology B: Microelectronics and Nanometer Structures Processing, Measurement, and Phenomena* **25**, 2558-2561 (2007).
- 29 Chen, F., Qing, Q., Xia, J., Li, J. & Tao, N. Electrochemical gate-controlled charge transport in graphene in ionic liquid and aqueous solution. *Journal of the American Chemical Society* **131**, 9908-9909 (2009).
- 30 Bard, A. J. & Faulkner, L. R. *Electrochemical methods Fundamentals and applications*. (John Wiley&Sons,Inc, 2001).
- 31 Das, A. *et al.* Monitoring dopants by Raman scattering in an electrochemically top-gated graphene transistor. *Nature Nanotechnology* **3**, 210-215 (2008).
- 32 Döppenschmidt, A. & Butt, H.-J. Measuring electrostatic double-layer forces on HOPG at high surface potentials. *Colloids and Surfaces A: Physicochemical and Engineering Aspects* **149**, 145-150 (1999).
- 33 Sun, S. *et al.* Phase reference in phase-sensitive sum-frequency vibrational spectroscopy. *The Journal of Chemical Physics* **144**, 244711 (2016).
- 34 Xu, X., Shen, Y. R. & Tian, C. Phase-sensitive sum frequency vibrational spectroscopic study of air/water interfaces: H₂O, D₂O, and diluted isotopic mixtures. *The Journal of Chemical Physics* **150**, 144701 (2019).

- 35 Tian, C. & Shen, Y. Structure and charging of hydrophobic material/water interfaces studied by phase-sensitive sum-frequency vibrational spectroscopy. *Proceedings of the National Academy of Sciences* **106**, 15148-15153 (2009).
- 36 Ji, N., Ostroverkhov, V., Tian, C. & Shen, Y. Characterization of vibrational resonances of water-vapor interfaces by phase-sensitive sum-frequency spectroscopy. *Physical review letters* **100**, 096102 (2008).
- 37 Wen, Y.-C. *et al.* Unveiling microscopic structures of charged water interfaces by surface-specific vibrational spectroscopy. *Physical Review Letters* **116**, 016101 (2016).
- 38 Cheng, J., Vermeulen, N. & Sipe, J. Second order optical nonlinearity of graphene due to electric quadrupole and magnetic dipole effects. *Scientific Reports* **7**, 1-11 (2017).
- 39 Somorjai, G. A. & Li, Y. *Introduction to surface chemistry and catalysis*. (John Wiley & Sons, 2010).
- 40 Lo Nostro, P. & Ninham, B. W. Hofmeister phenomena: an update on ion specificity in biology. *Chemical Reviews* **112**, 2286-2322 (2012).
- 41 Zhang, Y. *et al.* Doping-induced second-harmonic generation in centrosymmetric graphene from quadrupole response. *Physical Review Letters* **122**, 047401 (2019).
- 42 Wang, Y., Tokman, M. & Belyanin, A. Second-order nonlinear optical response of graphene. *Physical Review B* **94**, 195442 (2016).
- 43 Shin, S., Kang, H., Cho, D., Lee, J. Y. & Kang, H. Effect of electric field on condensed-phase molecular systems. II. Stark effect on the hydroxyl stretch vibration of ice. *The Journal of Physical Chemistry C* **119**, 15596-15603 (2015).
- 44 Tomlinson-Phillips, J. *et al.* Structure and dynamics of water dangling OH bonds in hydrophobic hydration shells. Comparison of simulation and experiment. *The Journal of Physical Chemistry A* **115**, 6177-6183 (2011).
- 45 Du, Q., Freysz, E. & Shen, Y. R. Surface vibrational spectroscopic studies of hydrogen bonding and hydrophobicity. *Science* **264**, 826-828 (1994).
- 46 Lu, G. & Zangari, G. Electrodeposition of platinum nanoparticles on highly oriented pyrolytic graphite. *Electrochimica Acta* **51**, 2531-2538, doi:10.1016/j.electacta.2005.07.038 (2006).
- 47 Zhao, G. & Liu, G. Electrochemical Deposition of Gold Nanoparticles on Reduced Graphene Oxide by Fast Scan Cyclic Voltammetry for the Sensitive Determination of As(III). *Nanomaterials (Basel)* **9**, doi:10.3390/nano9010041 (2018).

Acknowledgement: We thank discussions with Carbon Six. Co for the CVD graphene growth and Dr. Yu-Dan Su for the analysis of data. CST acknowledges support from the National Natural Science Foundation of China Grants (No. 12125403 and No. 11874123) and the National Key Research and Development Program of China (No. 2021YFA1400503 and No. 2021YFA1400202).

Author Contributions C.S.T conceived the project and designed the experiments. Y.X, SS. Y, YB. M and F. G and performed experimental data collection. C.S.T and Y. X wrote the manuscript.

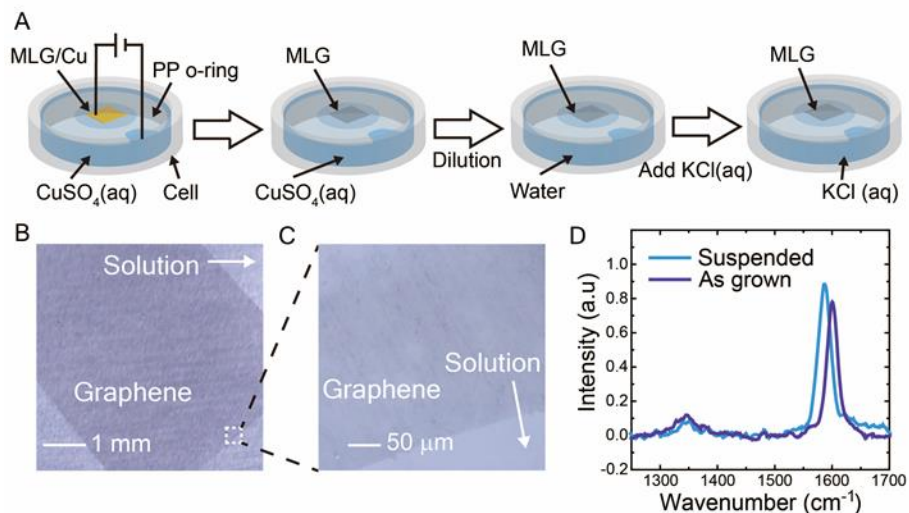


Fig. 1. Suspended MLG sample on water. **(A).** Fabrication process of the suspended MLG. The MLG on copper foil was put on the surface of CuSO_4 solution and a polypropylene (PP) O-ring was used to confine the sample in the central area of the cell. After etching copper substrate by electrolysis, the remaining electrolyte was diluted repeatedly with pure water, and then the supporting electrolyte KCl was added to reach 0.1 M. **(B).** Photograph of the MLG sample suspended on the electrolyte surface. **(C).** Enlarged microscope image of the sample in the white dashed box in **(B)**. **(D).** Raman spectrum of the suspended MLG sample compared to the graphene as-grown on the copper substrate.

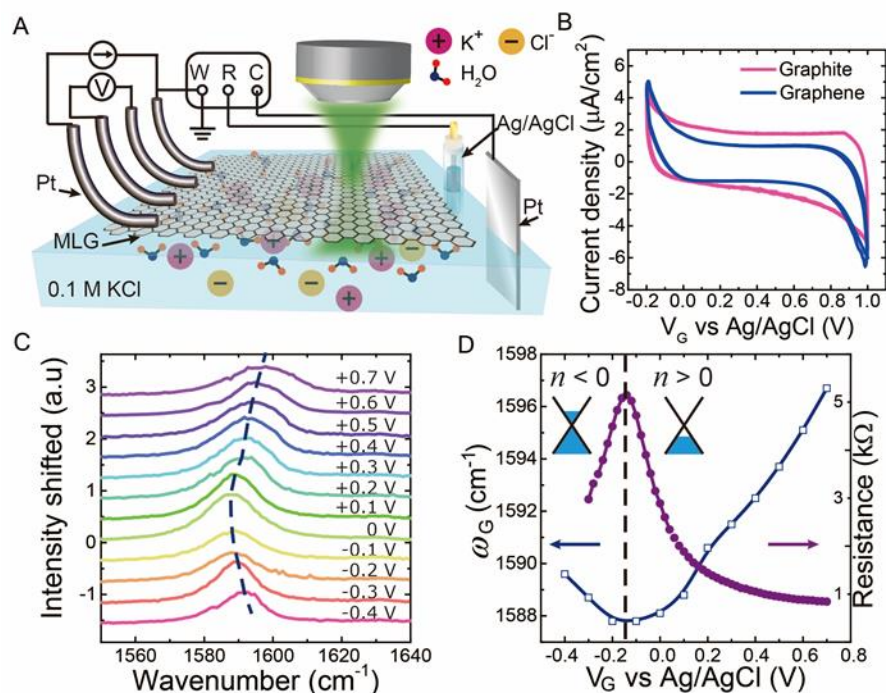


Fig. 2. Gate tunability of the suspended MLG. (A). Illustration of the gated MLG. Electronic circuit is sketched in the figure. W, R and C refers to working electrode, reference electrode and counter electrode, respectively. The four Pt wires ($\sim 20 \mu\text{m}$) are attached to the graphene, to perform four-probed resistance measurements and to tune the gate voltage (V_G). Raman scattering photons are excited and collected through the same objective. (B). CV scans on graphene and graphite. (C). Raman spectra of the MLG sample at different V_G . Dashed curve marks the frequency shift of the G-mode. (D). Shift of the G-mode (blue dots) and the resistance (purple dots) of MLG suspended on water versus gate voltage V_G . Curves serve as eye-guides. Inset illustrates the Dirac cone and Fermi level of graphene.

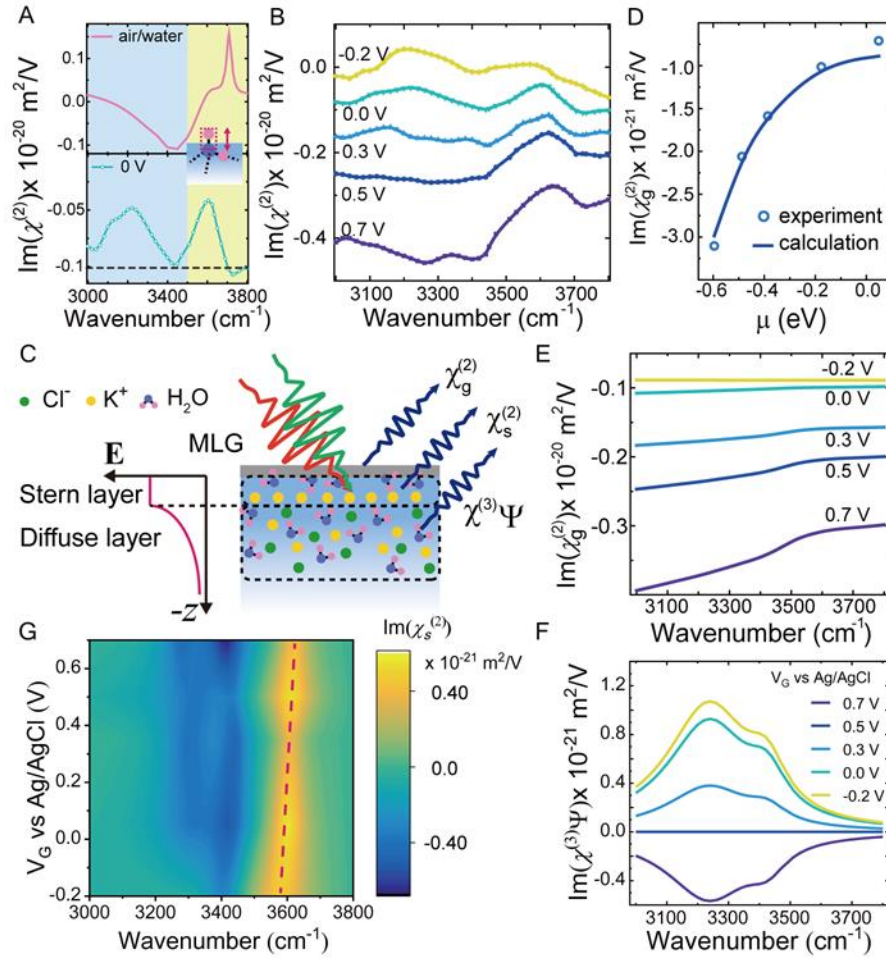


Fig. 3. In situ SFVS spectra of the graphene/electrolyte interface. (A). Comparison of $\text{Im}\chi^{(2)}$ spectrum at air/water interface and air/MLG/water interface. Inner plot illustrates the dangling O-H bond of water molecule protruding at the hydrophobic interface. (B). $\text{Im}\chi^{(2)}$ spectra at different V_G . (C). Illustration of the graphene/electrolyte interface with three origins contributing to the SF spectrum. The electric field distribution χ in the EDL is also sketched. (D). Theoretical and experimental data of $\text{Im}\chi_g^{(2)}$ at 3800 cm^{-1} versus chemical potential μ of graphene. (E). Calculated SF spectra of graphene ($\text{Im}\chi_g^{(2)}$) at different V_G . Fresnel factors have been taken into account (see SM for details). (F). Calculated SF spectra from the diffuse layer ($\text{Im}\chi^{(3)}\Psi$) at different V_G . (G). Contour plot of the Stern layer spectra ($\text{Im}\chi_s^{(2)}$) at different V_G . Red dashed line illustrates the frequency shift of the dangling O-H mode.

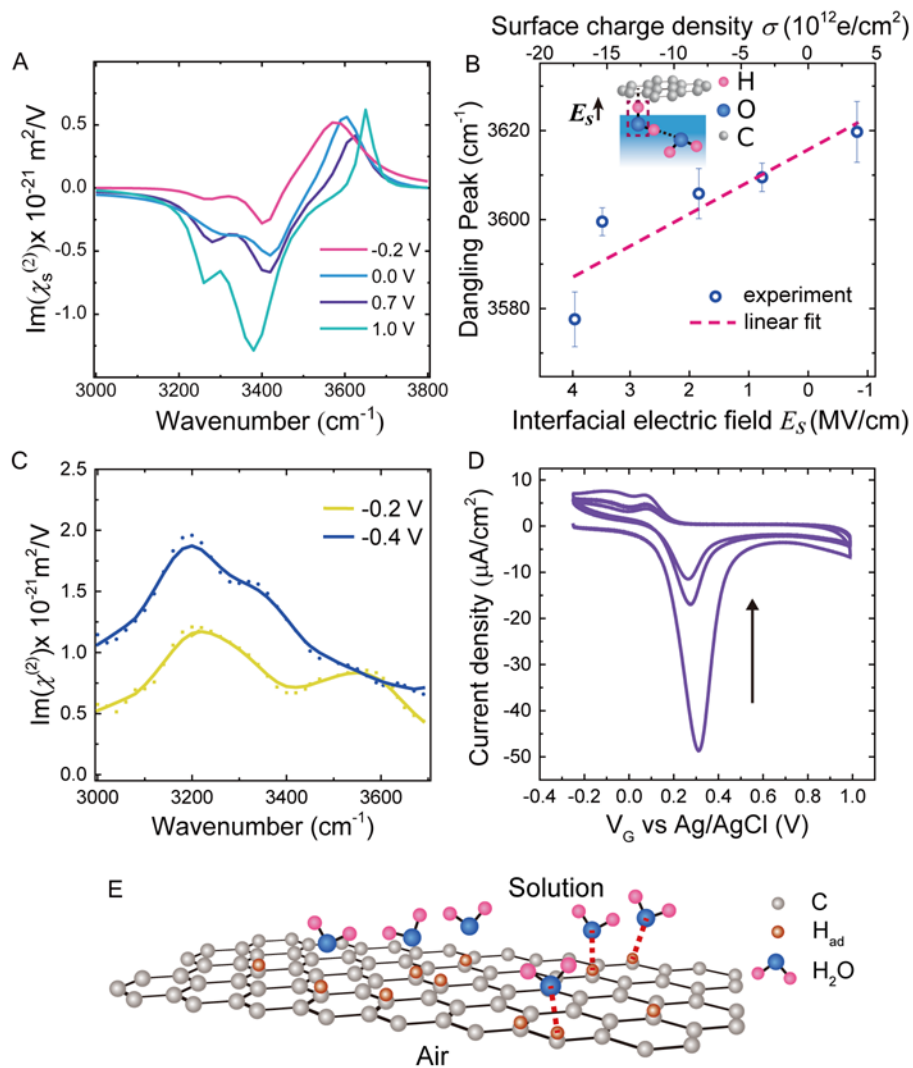


Fig. 4. SF spectrum and CV curves near the onset of chemical reactions. (A) Typical $\text{Im}\chi_s^{(2)}$ spectra from the Stern layer at different V_G . (B). Linear fit of the peak wavenumber of the dangling O-H mode. The interfacial electric field E_s would induce Stark shift of the dangling O-H mode (marked in the red dashed box) as illustrated in the inset. Black arrow: direction of positive E_s . (C). Comparison of $\text{Im}\chi^{(2)}$ (after subtraction of the graphene background) at $V_G = -0.4$ V and -0.2 V. Dots are experimental data and solid curves serve as eye-guides. (D). CV scans immediately after holding V_G at -0.4 V for ~ 4 hours. The black arrow indicates that the peak amplitude decreases after each loop. (E). Illustration of the adsorbed H atoms (H_{ad}) on

graphene, which would modify the hydrophobicity of graphene. The red dashed lines represent interactions between H_{ad} and water molecules, favoring the shown orientation of water molecules at the interface.